

# Abundances of four open clusters from solar stars. <sup>★</sup>

G. Pace<sup>1,2</sup>, L. Pasquini<sup>3</sup>, and P. François<sup>4</sup>

<sup>1</sup> Centro de Astrofísica, Universidade do Porto, Rua das Estrelas, 4150-762 Porto, Portugal

<sup>2</sup> Aryabhata Research Institute of Observational Sciences, Manora Peak, Nainital, 263129 Uttarakhand, India

<sup>3</sup> European Southern Observatory, Karl Schwarzschildstr. 2, Garching bei München, Germany

<sup>4</sup> Observatoire de Paris, 64 Avenue de l'Observatoire, 75014 Paris, France

Preprint online version: December 14, 2018

## ABSTRACT

**Aims.** We present abundance measurements of several elements (Fe, Ca, Na, Ni, Ti, Al, Cr, Si) for 20 solar-type stars belonging to four Galactic open clusters: NGC 3680, IC 4651, Praesepe and M 67. Oxygen abundances were also measured for most of the stars in each cluster but IC 4651. For NGC 3680 accurate abundance determination using high-resolution spectra covering a large spectral domain are computed for the first time.

**Methods.** We have used UVES high-resolution, high S/N ratio spectra and performed a differential analysis with respect to the sun, by measuring equivalent widths and adopting LTE hypothesis.

**Results.** The most surprising result is a significant supersolar metallicity for Praesepe ( $[\text{Fe}/\text{H}]=0.27\pm0.10$ ). As for the other clusters, we confirm a supersolar metallicity for IC 4651 ( $[\text{Fe}/\text{H}]=0.12\pm0.05$ ), a solar metallicity for M 67 ( $[\text{Fe}/\text{H}]=0.03\pm0.04$ ) and a slight undersolar metallicity for NGC 3680 ( $[\text{Fe}/\text{H}]=-0.04\pm0.03$ ). We find solar scaled abundances of almost all elements, with the notable exception of oxygen in NGC 3680 and Praesepe, supersolar in the former cluster ( $[\text{O}/\text{Fe}]=0.2\pm0.05$ ) and as low as  $[\text{O}/\text{Fe}]=-0.4\pm0.1$  in the latter. Observations of several objects per cluster is required to obtain robust results, especially for those elements with a limited number of suitable lines.

**Key words.** Open clusters: individual: – stars: abundances

## 1. Introduction

The last decade has seen an impressive effort devoted to better understand the chemical evolution of the Galaxy. On the theoretical side several new models have been created, that assume more complex (and likely more realistic) scenarios, for instance introducing two main in-fall episodes for the formation of the halo-thick disk and thin disk respectively (Chiappini et al. 1997, 2001; François et al. 2004), while, on the observational side, thanks to the performances achieved by the new-generation telescopes (VLT and Keck) and to the availability of multi-object spectroscopy, many high quality spectroscopic data have been gathered.

A longstanding question concerns the existence and the evolution of the chemical abundance gradient in the Galactic disk. Galactic open clusters probably represent the best tool for understanding whether and how the gradient slope changes with time, as they have formed at all epochs. Their distances are more accurate and less subject to observational biases with respect to other classes of objects.

Dias & Lépine (2005) located the birthplace of 612 open clusters and determined the spiral pattern rotation speed of the Galactic disk. The possibility of tracing open clusters back to where they formed is very interesting, since, coupled with metallicity measurements, it allows us to precisely reconstruct the chemical distribution of the Galactic disk also at past times. Dias & Lépine (2005) based their work on large photometric databases in the visible. They achieve important conclusions on the structure and dynamics of the spiral arms, but in order to precisely estimate the deviation of open cluster motions from circular orbits, and therefore improve the scale of Galactocentric distances at the place of birth, a more complete and precise database of age, distance, proper motion and radial velocity determinations is still required. The unprecedented opportunity provided by deep photometric surveys in the infrared, such as UKIDSS (Lawrence et al. 2007) and VISTA (McPherson et al. 2006), opens exciting perspectives: they could be used to create deep, complete, precise and homogeneous open cluster database of location in the 3-D space, age and reddening. The calibration of photometric metallicity indicators could be used for the clusters not observable with high-resolution spectroscopy.

Open clusters have the further advantage of providing a sample of coeval stars that formed from the same material, which means, in particular for main-sequence stars, that they should have the same atmospheric chemical composition. As a result, the chemical composition of an open cluster can be studied through several stellar spectra. With all these advantages, clearly open clusters are ideal objects to probe the chemical evolution of the Galactic disk. Of course a large sample is required, spanning as broad a range of Galactocentric distances and ages as possible.

---

*Send offprint requests to:* G. Pace, e-mail: [gpace@aries.ernet.in](mailto:gpace@aries.ernet.in)

\* Observations collected at the ESO VLT. Table 1 is only available in electronic form at the CDS via anonymous ftp to [cdsarc.u-strasbg.fr](ftp://cdsarc.u-strasbg.fr) (130.79.128.5) or via <http://cdsweb.u-strasbg.fr/cgi-bin/qcat?J/A+A/>

Finally, clusters are at the basis of our understanding of stellar evolution, and clean clusters colour–magnitude diagrams, having well determined abundances, can be used to test directly stellar evolution models (see e.g. Nordstroem et al. 1997).

At the end of the last decade, not many open clusters had accurate chemical composition determined from high-resolution spectra of several stars, and these were mainly studied by observing few of their giant stars (Gratton 2000). The situation is rapidly evolving in particular thanks to coordinated efforts which uses new facilities available at 8-M-class telescopes (Randich et al. 2005; Bragaglia & Tosi 2006). This work joins several recent contributions to the effort of establishing a robust open-cluster metallicity scale. In the past, random and systematic errors gave rise to – sometimes dramatic – discrepancies in abundance determinations of a given open cluster as computed from different groups. We confirm that this is no longer the case when comparing independent metallicity measurements from high resolution spectroscopy.

## 2. Observations and data reduction

The data used were primarily collected to study the chromospheric activity evolution of solar-type stars (Pace & Pasquini 2004). The sample includes two stars in NGC 3680, five in IC 4651, seven in Praesepe and six in M 67. The targets were chosen to be on the main sequence, high-probability members of the clusters and not known to be binaries at the time of the observations. The choice was done using as references Nordstroem et al. (1996) for NGC 3680, Meibom et al. (2002) for IC 4651 and several sources for M 67, including Latham et al. (1992) for the binary determination in this cluster. From the sample originally collected and used in Pace & Pasquini (2004), one M 67 star has been excluded because it turned out to be a binary (Randich et al. 2006). Our stars have colours comprised within  $0.51 < (B-V)_0 < 0.72$ , closely encompassing the solar colour which is evaluated around  $B-V = 0.65$  (see e. g. Pasquini et al. 2008). We also note that the paucity of stars observed in NGC 3680 is imposed by the fact that, as shown by Nordstroem et al. (1997), this cluster has very few single G stars members left, most of its low mass members being dispersed in its lifetime.

Star names are taken from Eggen (1969) for NGC 3680, Anthony-Twarog et al. (1988) and Eggen (1971) for IC 4651, Sanders (1977) for M 67, Klein Wassink (1927) for Praesepe.

The spectra were obtained in the ESO observing run 66.D-0457 with the UVES spectrograph at the focus of Kueyen 2 of the VLT (Dekker et al. 2000). While the blue part of the spectra was used mainly to determine the level of chromospheric activity, we recorded simultaneously red spectra, in the range between 480 and 680 nm. Given the higher flux of the stars in this range, we could narrow the UVES red slit to 0.4 arcseconds, to obtain in the red range a resolution of  $R=100\,000$ , still keeping a high S/N ratio in this domain. With some variation from star to star and from the different regions of the spectra, the S/N ratio/pixel is about 130 for Praesepe stars and 80 for the others. The spectra have been reduced with the UVES pipeline (Modigliani et al. 2004), and then analysed both with MIDAS and IDL routines

### 3. Abundance analysis

Abundance measurements were carried out by measuring equivalent widths (EWs) and using OSMARCS models (Edvardsson et al. 1993), in a standard-LTE analysis. We have used the line list from Randich et al. (2006), out of which suitable lines in the EW-range 5–140 mÅ were selected. EW measurements were performed by using an IDL program made by one of the authors (G. P.), which works in a semi-automatic fashion, allowing a visual control of the fit of each selected line.

We first went through the chemical analysis of the Sun, using the EW measurements made in Randich et al. (2006), and the well-known values for temperature and gravity (see e.g. Stix 2002). The solar EW measurements used are made on an UVES spectrum at a resolution of  $R=45\,000$ . A comparison with EW measurements on the UVES archive solar spectrum with the same configuration as our sample spectra, showed that difference of resolution power from  $R=45\,000$  to  $R=100\,000$  does not have any detectable effect on the EWs, therefore we preferred to employ published measurements. We have tried several values for the microturbulence and eventually chosen the one giving the flattest trend in the EW vs. abundance diagram, namely 1.1 km/sec. The results, line by line, are available at the CDS in form of electronic Table (Table 1) containing the following information. Column 1 lists the wavelength, Column 2 gives the element’s chemical symbol, Column 3 the ionization stage, Column 4 indicates the EW measurement, Column 5 gives the resulting chemical abundance. While the correlation coefficient between  $[\text{Fe}/\text{H}]$  and EW is very close to 0, namely 0.02, that between  $[\text{Fe}/\text{H}]$  and the excitation potential ( $\chi$ ) is -0.42, and the difference between Fe I and FeII is of -0.05 dex. These numbers are significantly different from zero. Small inaccuracies of the model in reproducing the atmospheric temperature stratification, rather than the limits of the LTE assumption, could be responsible for the slope in the  $[\text{Fe}/\text{H}]$  vs.  $\chi$  diagram and for a poor ionization equilibrium, since lines with different excitation potential tend to form in different layers of the solar atmosphere (Grevesse & Sauval 1999).

By performing a differential analysis line by line with respect to the Sun, we expect to greatly reduce the spurious trends and to restore the ionisation equilibrium when evaluating the stellar parameters, provided that the structure of the stellar photosphere does not differ too much from the solar one, which is a reasonable assumption since our targets are solar-type stars.

For all the sample stars, atmospheric parameters that best reproduce excitation and ionisation equilibria were selected from a broad grid of guess values.

The temperature estimates around which the grids were built, were computed on a first approximation based on the existing photometry, using V-H, V-J and V-K colours. V-magnitudes have been taken from the reference papers in Section 2 for IC 4651, from Nordstroem et al. (1997) for NGC 3680, from Montgomery et al. (1993) for M 67, and from Jones & Stauffer (1991) for Praesepe, with the exception of KW 368 and KW 208, whose V-magnitudes are taken instead from, respectively, Jones & Cudworth (1983) and Johnson (1952). We have then adopted J, H and K magnitudes from the 2 MASS catalogue (Skrutskie et al. 2006). Each of the V-H, V-J and V-K colours were then transformed into

X	A(X) <sub>our</sub>	A(X) <sub>litt</sub>	Number of lines	$\sigma$
FeI	7.52	7.50	66	0.03
FeII	7.57	7.50	11	0.03
NaI	6.37	6.33	3	0.11
AlI	6.47	6.47	2	0.02
SiI	7.56	7.55	9	0.03
CaI	6.36	6.36	11	0.03
TiI	4.97	5.02	11	0.02
CrI	5.65	5.64	6	0.06
NiI	6.25	6.25	23	0.04

**Table 2.** Comparison between our solar abundances (second Column) and those by Grevesse & Sauval (2000) (third Column). For iron, the abundance value obtained using ionised lines is also given. The number of lines and the standard deviation of the measurements for each species are also reported in the fourth and in the fifth Column respectively. When only three or two lines are measured (sodium and aluminum), half of the difference between the maximum and minimum value is reported instead of the standard deviation.

a temperature estimation using Ramírez & Meléndez (2005), and the three values were averaged.

The comparison between photometric and spectroscopic temperatures indicates that the colour-colour and colour-temperature transformations could be affected by some systematics, and that the colour excess adopted for IC 4651 could be underestimated (see Section 4.4).

As for gravity, we have used the values expected for a dwarf according to: 1) the previously determined photometric temperature; 2) the stellar ages, i.e. those of the parent cluster given in Carraro & Chiosi (1994) and, only for Praesepe, in the WEBDA database; and 3) the solar metallicity isochrones by Girardi et al. (2000).

Microturbulence were left free to vary in the range from  $\approx 0.7$  to  $\approx 1.7$  km/sec.

Temperature, gravity and microturbulence velocity were set equal to those values for which no significant trend of the computed iron abundances is present, neither as a function of the excitation potential of the line nor as a function of its EW, and for which the iron abundances obtained respectively with Fe I and Fe II lines give equal results within the errors. The correlation coefficients of EW vs. abundance and  $\chi$  vs. abundance are generally *approx* 0.1 or smaller, always smaller than 0.3 and Fe I and FeII give results always in agreement within 0.03 dex. Praesepe stars are an exception in that we did not manage to find parameters as good as those found for the other stars and compatible with the photometric data, and we have in some cases accepted correlation coefficients as high as 0.5. The explanation for this is that we have used the same line list for all the sample, therefore Praesepe stars, which are more metal rich thus having an EW range shifted towards larger values, which means a higher percentage of lines close to saturation and fewer weak lines, hence a less constrained microturbulence. Furthermore microturbulence

is significantly higher in Praesepe stars than in the others. Possibly some differences in the structure of the photosphere due to the higher metallicity and rotation velocity, could lead to a higher microturbulence. In any case, as we will see, the conclusion of a significantly higher chemical abundance for these stars is very robust.

For each tentative combination of temperature, gravity and microturbulence values of the grid, the metallicity was initially set to solar, and then iteratively substituted with the average abundance resulting from Fe I lines, until convergence was obtained. Furthermore, for each measured line, the abundances were calculated differentially with respect to the sun. This, in addition to the already mentioned better parameter determination, allows us to compensate for errors in the  $\log gf$  values (Langer et al. 1998).

The steps of the grid values are 20 K for the temperature, 0.02 dex for  $\log G$  and 0.02 km/sec for  $\xi$ . This check has been made with fiftyfour to sixtyfour Fe I and nine to eleven Fe II lines in each star. Only in three Praesepe stars no more than seven or eight Fe II lines could reliably be measured, and in one of them no more than fortytwo Fe I lines.

As expected, we found a correlation between microturbulence and temperature obtained as described above. Praesepe stars, as already discussed, have a significantly higher microturbulence value, therefore we have calibrated two different linear T-vs.- $\xi$  relationship, one for Praesepe, one for the rest of the stars.

We have fine tuned the parameters, in order to make  $\xi$  as close as possible to the value expected according to the calibrations, and the gravity as consistent as possible with the spectroscopic temperature, not anymore with the photometric one.

We have calibrated the T-vs.- $\xi$  relationship for the second time, with the finally adopted parameters, not using Praesepe stars. The result is:

$$\xi = -5.42 + 6.30 \cdot \frac{T_{eff}}{T_{\odot}}, \quad \sigma = 0.06$$

$\sigma$  being here the standard deviation of the datapoints around the fit. For the remainder of the paper we will refer as  $\xi_{fit}$  to the microturbulence values derived from the fit above.

Abundances were finally recomputed assuming the fine tuned parameters.

We have measured in cluster stars the abundance of oxygen, which is treated separately, iron, calcium, aluminum, sodium, nickel, titanium, chromium and silicon. Similarly to what we have done with iron lines, we have used solar measurements as reference value for all our [X/H] estimates in the cluster stars, computing for all elements the difference between the stellar and the solar value line by line.

Oxygen abundances, instead, were derived from measured EWs of the O I 6300.30 Å forbidden line employing the same method used by Randich et al. (2006). Namely, we employed MOOG (Sneden 1973, version 2002) and Kurucz model atmosphere (Kurucz 1993). We used the driver *blend* that allows taking into account the contribution of the blending Ni I 6300.34 feature when force fitting the abundance of the O to the measured EWs of the 6300.3 Å feature. As input to MOOG we used stellar parameters and iron and nickel abundances determined by our analysis. For the oxygen and nickel lines we employed  $gf$ -values equal  $\log gf = -9.717$  and  $\log gf = -2.11$ , respectively, following Allende Prieto et al. (2001) and Johansson et al. (2003) (see Randich et al. 2006, for additional details).

Thanks to the cluster radial velocities we did not need to correct for the presence of telluric lines for NGC 3680, Praesepe and M 67; on the other hand, telluric lines were

severely affecting the spectra of IC 4651 stars, and we were not able to correct for them due to unavailability of suitable standard stars. Finally, for three stars in Praesepe and one in M 67 we were not able to measure the O I line.

#### 4. The results

The results for the Sun are summarised in in Table 2, those for the cluster stars in Table 3.

The results shown in Table 2 are obtained with the ( $T=5780$ ,  $G=4.40$ ,  $\xi=1.1$ ) model. In the first Column element and ionization stage are indicated. In the second Column we wrote our results, and in the third the values from Grevesse & Sauval (2000) are given as comparison.

For each star the mean abundance values of all the elements studied but oxygen are given in Table 3, along with the error resulting from the analysis described in Section 4.1. The standard deviation resulting from the measurements of the different lines, and the number of lines measured for each element are also given (when no more than three lines could be measured, half the difference between the highest and lowest values is given instead of the standard deviation). All the values refer to the neutral-element lines. The stars are grouped by cluster, and for each cluster one abundance is obtained by averaging the abundance of all stars. The relative standard deviation is also computed, but for NGC 3680, which has only 2 stars observed. In this case the half difference between the two stellar abundances is given. These standard deviations well indicate the robustness of our analysis. Only in four cases, namely aluminum in Praesepe and M 67 and titanium and chromium again in M 67, the cluster abundance dispersion is larger than 0.07 dex. Furthermore, we have to notice that the dispersion in M 67 stellar abundances is significantly enhanced by Sanders 1287, which always shows the lowest chemical content. Its case is worth further investigation. On the other hand the maximum difference among stars belonging to the same cluster can be easily larger than 0.1 dex, which calls for caution when deriving conclusions based on a small number of objects. As errors on the final values we use the standard deviations of the stellar abundance measurements in each cluster.

Since for Praesepe, in the parameter determination, higher  $EW-[Fe/H]$  and  $\chi-[Fe/H]$  correlations sometimes remain, we take the more conservative average error estimate for its single stars coming from the analysis described in Section 4.1: 0.10 dex. By doing so we account for the possibility of a systematic component in the parameter determination of Praesepe stars.

##### 4.1. Errors

There are three sources of measurement errors in our abundance analysis:

- errors on EW measurements;
- errors on atmospheric parameters;
- errors on  $\log gf$  values.

The last item is the least important, since it should mostly cancel out when subtracting the stellar abundances from the solar ones. EW measurements and atmospheric-parameter

determinations, on the other hand, are subject to errors that do not necessarily cancel out in the stellar and the solar estimations.

#### 4.1.1. Errors on equivalent width measurements and $\log gf$

Errors on EW measurements are mostly due to the uncertainty in the choice of the continuum, therefore we would greatly underestimate them by using the Cayrel formula (Cayrel et al. 1988). They are by far the major contributors to the dispersion of the abundance measurements from different lines of the same element. The latter value, divided by the square root of the number of lines, has to be quadratically added to the other contributions to eventually compute the global error.

#### 4.1.2. Errors on the parameter atmosphere

To evaluate the uncertainty in the parameters, we have used the differences between those derived in our spectral analysis – namely  $T_{spec}$ ,  $G_{spec}$  and  $\xi_{spec}$  – and the computed ones:  $T_{phot}$ ,  $G_{phot}$  and  $\xi_{fit}$ . The evaluations of  $T_{phot}$  and  $G_{phot}$  and the linear regression used to compute  $\xi_{fit}$ , have been discussed in Section 3. The uncertainty in the gravity was calculated as the quadratic average (equal to the standard deviation) of  $G_{spec} - G_{phot}$ . As for  $\xi$ , we proceeded in a similar way, adopting the rms of the  $\xi_{spec} - \xi_{fit}$  differences. We remind the reader that the linear fit giving  $\xi_{fit}$  as a function of the temperature has been computed without using Praesepe stars. For them, the uncertainty in the microturbulence, which is higher, has been computed separately, though by means of the same formula.

As for the temperature, we have used a slightly modified approach because by proceeding in the same way one would overestimate the uncertainty on temperature and ignore errors in the reddening, which may also contribute to the differences  $T_{spec} - T_{phot}$ . So we have computed the mean value of  $T_{spec} - T_{phot}$  for each cluster, and we have assumed that such mean value arises from a wrong evaluation of the reddening. Therefore only after removing it from each term have we proceeded in evaluating the standard deviation of  $T_{spec} - T_{phot}$ .

The final values for the uncertainty in the parameters turn out to be:

$$\Delta T = 110 \text{ K}, \Delta G = 0.07 \log(\text{gr}\cdot\text{cm}\cdot\text{sec}^{-2}), \Delta \xi = 0.06 \text{ km}\cdot\text{sec}^{-1}, \\ \Delta \xi = 0.18 \text{ km}\cdot\text{sec}^{-1} \text{ for Praesepe}$$

#### 4.1.3. Errors on the final abundance values.

In order to evaluate the uncertainty in the final abundance caused by the error on a given atmospheric parameter ( $T_{eff}$ ,  $\log G$  or  $\xi$ ), we have repeated the whole chemical analysis twice, once enhancing its value and once diminishing it by an amount equal to its error, computed as described in Section 4.1.2. While doing this, all the other parameters have been kept constant. Then we have done the same for the errors on the EW measurements and  $\log gf$  (see Section 4.1.1) and we have finally added quadratically all the contributions.

However, as discussed above, we believe that a better estimate of our final errors on the abundances given are represented by the standard deviation values. The abundance mea-



measurements of different stars belonging to the same cluster actually represent independent evaluations of the same quantity, which is the cluster abundance. The error analysis in this Section is meant to find out what parameters most influence the final determination, and check whether our method for evaluating such parameters is robust.

We find that temperature dominates the final error, being the other contributions in most cases marginal or even negligible, and that the assumed uncertainty of 110 K, which results from the differences between spectroscopic and photometric evaluation, seems to slightly overestimate the errors.

As for EW, even though for a single line the measurement error can sometimes reach up to  $\sim 20\%$ , having at disposal many lines renders its contribution to the total error far less important than the uncertainty in the temperature.

According to these tests, silicon is more insensitive than other elements to the uncertainties. It is quite remarkable as, in Table 3, the [Si/H] dispersion in the measurements of each cluster is among the smallest, being indeed the smallest one for IC 4651 and NGC 3680 despite the small number of the lines used. This would again point towards a very good consistency in our analysis.

CLUSTER	$ \frac{\partial[Fe/H]}{\partial\xi} \cdot \Delta\xi $	$ \frac{\partial[Fe/H]}{\partial T} \cdot \Delta T $	$ \frac{\partial[Fe/H]}{\partial G} \cdot \Delta G $	$ \frac{\partial[Fe/H]}{\partial EW} \cdot \Delta EW $	
NGC 3680	0.01	0.09	0.01	<0.01	
IC 4651	0.02	0.09	0.01	<0.01	
PRAESEPE	0.06	0.09	0.01	<0.01	
M 67	0.02	0.09	0.01	<0.01	
	$ \frac{\partial[Na/H]}{\partial\xi} \cdot \Delta\xi $	$ \frac{\partial[Na/H]}{\partial T} \cdot \Delta T $	$ \frac{\partial[Na/H]}{\partial G} \cdot \Delta G $	$ \frac{\partial[Na/H]}{\partial EW} \cdot \Delta EW $	$ \frac{\partial[Na/H]}{\partial met} \cdot \Delta met $
NGC 3680	<0.01	0.05	0.01	0.01	0.01
IC 4651	0.01	0.06	0.01	0.02	0.01
PRAESEPE	0.02	0.06	0.01	0.02	0.01
M 67	0.01	0.06	0.01	0.01	0.01
	$ \frac{\partial[Ni/H]}{\partial\xi} \cdot \Delta\xi $	$ \frac{\partial[Ni/H]}{\partial T} \cdot \Delta T $	$ \frac{\partial[Ni/H]}{\partial G} \cdot \Delta G $	$ \frac{\partial[Ni/H]}{\partial EW} \cdot \Delta EW $	$ \frac{\partial[Ni/H]}{\partial met} \cdot \Delta met $
NGC 3680	0.01	0.06	<0.01	0.01	0.01
IC 4651	0.01	0.06	<0.01	0.01	0.01
PRAESEPE	0.03	0.06	<0.01	0.01	0.01
M 67	0.01	0.06	<0.01	0.01	0.01
	$ \frac{\partial[Si/H]}{\partial\xi} \cdot \Delta\xi $	$ \frac{\partial[Si/H]}{\partial T} \cdot \Delta T $	$ \frac{\partial[Si/H]}{\partial G} \cdot \Delta G $	$ \frac{\partial[Si/H]}{\partial EW} \cdot \Delta EW $	$ \frac{\partial[Si/H]}{\partial met} \cdot \Delta met $
NGC 3680	< 0.01	0.02	<0.01	0.01	0.01
IC 4651	< 0.01	0.02	<0.01	0.01	0.01
PRAESEPE	0.01	0.02	<0.01	0.02	0.02
M 67	< 0.01	0.02	<0.01	0.01	0.02

**Table 4.** Table of the typical errors associated with abundance measurements of iron (about sixty Fe I lines), sodium (two or three lines) and nickel (about twenty lines).

Star	EW 6300.30 Å (mÅ)	n(O)	[O/Fe]
AHTC 1009	7.0 ±1	8.91 ±0.09	0.25 ± 0.13
Eggen 70	4.7 ±0.8	8.75 ±0.07	0.16 ± 0.11
NGC 3680		8.83 ±0.08	0.20 ± 0.05
KW 100	–	–	–
KW 208	–	–	–
KW 326	5.4 ±0.8	8.51 ±0.17	−0.44 ± 0.20
KW 368	5.0 ±0.8	8.40 ±0.17	−0.52 ± 0.20
KW 392	4.8 ±0.5	8.69 ±0.10	−0.32 ± 0.15
KW 418	4.0 ±1	8.48 ±0.20	−0.42 ± 0.22
KW 49	–	–	–
PRAESEPE		8.52 ±0.12	−0.42 ± 0.08
Sanders 1048	4.4 ±0.6	8.49 ±0.09	−0.20 ± 0.13
Sanders 1092	4.5 ±1.5	8.67 <sup>+0.19</sup> <sub>−0.32</sub>	−0.06 <sup>+0.21</sup> <sub>−0.33</sub>
Sanders 1255	5.3 ±0.4	8.68 ±0.06	0.01 ± 0.12
Sanders 1283	–	–	–
Sanders 1287	4 ±1	8.58 <sup>+0.14</sup> <sub>−0.19</sub>	−0.04 <sup>+0.17</sup> <sub>−0.21</sub>
Sanders 746	5.3 ±0.7	8.65 ±0.1	−0.08 ± 0.13
M 67		8.61 ±0.08	−0.07 ± 0.08

**Table 5.** EWs of the 6300.30 Å O I line derived oxygen abundances. In both columns the global cluster errors for the cluster refer to the standard deviations of the abundances coming from the single stars, while reported errors on single star abundance measurements come from the uncertainty in the EWs. See the text for the errors due to the parameter uncertainty.

#### 4.2. Oxygen

Measured EWs of the 6300.30 Å line, together with derived n(O) and [O/Fe] values are listed in Table 5. We recall from Randich et al. (2006) that using the same method and log-*gf* values we derive a solar oxygen abundance  $n(\text{O})_{\odot}=8.66$ .

Listed errors in n(O) values include the contribution of uncertainties in the measured EWs of the forbidden line and errors in Ni abundances (which are, however, negligible). Uncertainties in stellar parameters, i.e.  $\Delta T = \pm 110$  K,  $\Delta G = \pm 0.07$  dex, and  $\Delta \xi = \pm 0.06$  km/s, reflect respectively into  $\Delta n(\text{O}) = -0.08/0.05, \pm 0.04$ , and  $\pm 0.02$ . The uncertainty of  $\pm 0.19$  km/s for the microturbulence velocity in Praesepe stars, reflects, instead, into  $\Delta n(\text{O}) = 0.06/-0.07$ .

Based on a single, faint line, these measurements suffer of some considerable uncertainty. On the other hand the average value for each cluster has a standard deviation smaller than the typical uncertainty in the [O/Fe] estimation of each single star.

#### 4.3. Comparison with published data

In this Section we are going to summarize the published data about chemical abundances in our target clusters, and compare them with our results. The content of the Section is

summarized in Table 6, in which we ignore photometric and low-resolution spectroscopy studies. We add the data compilation for Collinder 261, NGC 6253 and Berkeley 29, which have been studied twice, to compare results independent chemical analysis and verify the overall reliability of abundance measurements from high-resolution spectroscopy.

[Fe/H]	[O/Fe]	[Al/Fe]	[Ni/Fe]	[Na/Fe]	[Si/Fe]	[Ca/Fe]	[Ti/Fe]	N	Reference	R	Instr/OBS
IC 4651											
0.12±0.05	–	-0.10±0.06	-0.02±0.08	-0.03±0.07	-0.02±0.05	0.04±0.06	-0.02±0.07	4	1	100K	UVES/VLT
0.11±0.01	–	–	–	–	–	–	–	5	4	48K	FEROS/1.5m
0.10±0.03	–	0.01±0.07	0.05±0.05	0.02±0.16	0.07±0.03	0.02±0.04	0.09±0.04	22	10	100K	UVES/VLT
Praesepe											
0.27±0.10	-0.4 ±0.2	-0.05±0.12	-0.02±0.10	-0.04±0.12	-0.01±0.12	0.00±0.11	-0.04±0.12	7	1	100K	UVES/VLT
0.04±0.04	–	–	–	–	–	–	–	7	7	60&30K	CFHT & Hale
0.11±0.03	–	–	–	–	–	–	–	4	2	55K	MIKE/MagCl
M 67											
0.03±0.04	-0.07±0.08	-0.03±0.11	-0.02±0.07	-0.02±0.07	-0.03±0.06	0.03±0.07	-0.02±0.11	6	1	100K	UVES/VLT
0.02±0.14	0.07±0.03	0.17±0.05	0.08±0.10	0.30±0.10	0.09±0.11	0.07±0.06	0.12±0.07	3	14	28K	KPNO & CTIO
0.03±0.03	0.01±0.03	-0.05±0.04	-0.02±0.04	0.05±0.07	0.02±0.04	0.05±0.04	-0.02±0.04	10	11	45K	UVES/VLT
-0.03±0.03	0.02±0.04	0.14±0.06	0.04±0.06	0.19±0.07	0.10±0.04	0.04±0.08	0.04±0.10	12	13	60&30K	SOFIN/NOT
0.02±0.12	–	–	–	–	–	–	–	3	7	60K	CFHT
-0.04±0.12	–	–	–	–	–	–	–	8	9	34K	KPNO
Collinder 261											
-0.03±0.03	-0.2 ±0.1	0.12±0.08	0.06±0.08	0.33±0.06	0.24±0.05	0.01±0.05	-0.12±0.09	6	5	48K	FEROS/1.5m
-0.22±0.11	-0.1 ±0.15	0.39±0.12	0.02±0.04	0.48±0.22	0.22±0.09	-0.04±0.10	-0.07±0.09	7	8	25K	CTIO
Be 29											
-0.54±0.02	0.23±0.03	0.26±0.01	-0.02±0.02	0.36±0.01	0.18±0.02	0.02±0.02	0.33±0.04	2	14	28K	KPNO & CTIO
-0.44±0.18	0.18±0.02	0.20±0.03	0.11±0.06	0.39±0.08	0.22±0.03	0.10±0.06	0.02±0.01	2	3	34K	HIRES/KECK
NGC 6253											
0.46±0.03	-0.18±0.06	-0.08±0.12	-0.05±0.01	0.21±0.02	0.09±0.06	-0.02±0.12	-0.19±0.10	4	6	43K	UVES/VLT
0.36±0.07	–	–	0.08±0.07	–	0.02±0.08	-0.04±0.12	-0.01±0.14	5	12	47K	UVES/VLT

**Table 6.** Literature data about high-resolution spectroscopic studies for clusters that have more than one high-resolution entry. Errors refer to the rms dispersion between stellar values, or half of the full spread when only two or three stars are studied. From Column 1 to Column 8 we show the abundance measurements. In Column 9 the number of stars used is given, in Column 10 the reference, in Column 11 and Column 12 we indicate, respectively, the spectral resolution and the instrument and/or the observatory.

References (1)Present study; (2)An et al. (2007); (3)Carraro et al. (2004); (4)Carretta et al. (2004); (5)Carretta et al. (2005); (6)Carretta et al. (2007); (7)Friel & Boesgaard (1992); (8)Friel et al. (2003); (9)Hobbs & Thorburn (1991); (10)Pasquini et al. (2004); (11)Randich et al. (2006); (12)Sestito et al. (2007); (13)Tautvaišienė et al. (2000); (14)Yong et al. (2005).

#### 4.3.1. NGC 3680

Anthony-Twarog & Twarog (2004) found for this cluster  $[\text{Fe}/\text{H}] = -0.14 \pm 0.03$ , thus corroborating the result found by Pasquini et al. (2001):  $[\text{Fe}/\text{H}] = -0.17 \pm 0.12$ . The former analysis is based on CCD photometry on the intermediate-band  $uvby\text{CaH}\beta$ , the latter on a small portion of a high dispersion spectrum of a single giant.

Friel et al. (2002) published radial velocities and metallicities for a sample of 39 clusters older than the Hyades. They used spectra at a resolution of 4 Å FWHM. We have two clusters included in their target list: M 67 and NGC 3680, for which they give  $[\text{Fe}/\text{H}] = -0.15$  and  $-0.19$  dex respectively, with a standard error of 0.05 dex for both. They had 25 stars in M 67 and 7 in NGC 3680. The difference with our result is significant, but both our and Friel et al.'s measurements point to a difference of about 0.05 dex between the two clusters, NGC 3680 being more metal poor. The disagreement with the value given by Nordstroem et al. (1997) for NGC 3680, namely  $[\text{Fe}/\text{H}] = +0.11$ , based on  $uvby\beta$  photometry, is beyond measurement errors.

Our result of a slight metal-poor composition ( $[\text{Fe}/\text{H}] = -0.04 \pm 0.03$ ) is the first one to our knowledge based on high-resolution spectra of a wide wavelength range.

#### 4.3.2. IC 4651

Also for IC 4651 several recent values of metallicity are available. Pasquini et al. (2004) based their results also on UVES spectra. They observed twenty stars, including both dwarfs and giants. A particular effort was made to sample the region around the turn off. They measured an iron abundance of  $[\text{Fe}/\text{H}] = 0.10 \pm 0.03$ , in excellent agreement with ours. Carretta et al. (2004) observed 4 clump stars with the high-resolution spectrograph FEROS at the focus of the ESO 1.5-meter telescope, and they found  $[\text{Fe}/\text{H}] = 0.11 \pm 0.01$ . Also in this case the agreement on the iron content is excellent, and it is remarkable that the same iron content is found for giants and dwarfs. Meibom et al. (2002) also found  $[\text{Fe}/\text{H}] = 0.1$  dex. Their result is based on  $uvby\beta$  photometry. The  $[\text{Fe}/\text{H}]$  content of this cluster seems therefore amazingly well established and agreed by all recent works.

As far as other elements are concerned, a comparison can be done with Pasquini et al. (2004) who measured abundances for several elements in common to us. The results they obtain for main sequence stars are in very good agreement (within 0.03 dex) with ours as far as calcium, aluminum, and nickel are concerned. The discrepancy of sodium abundances is also within the error (0.06 dex, roughly  $1\sigma$ ). For the remaining elements (silicon, titanium and chromium) the difference ranges from 0.09 to 0.11 dex. Note that, while we have considered here only data about main-sequence stars, the values given in Table 9 regarding

Pasquini et al. (2004) refer to the overall cluster abundance, and the agreement turns out to be worse. Within  $\approx 2\sigma$ , all the results show a substantial solar-scaled mixture.

#### 4.3.3. M 67

Tautvaišienė et al. (2000) have obtained for this cluster  $[\text{Fe}/\text{H}] = -0.03 \pm 0.03$  by analysing evolved stars, among which also helium core-burning stars of the clump. Hobbs & Thorburn (1991) found  $[\text{Fe}/\text{H}] = -0.04 \pm 0.12$ . A very similar value, i.e.  $[\text{Fe}/\text{H}] = -0.05$ , has been found using calibrations of the ultraviolet excess at  $(B - V)_0 = 0.06$  as a function of  $[\text{Fe}/\text{H}]$  (Montgomery et al. 1993). Friel & Boesgaard (1992) collected spectra at a resolution of  $0.25 \text{ \AA}$  for three M 67 dwarf stars, with  $[\text{Fe}/\text{H}]$  values of  $-0.07$ ,  $0.05$  and  $0.03$ . Yong et al. (2005) collected spectra at a resolution of 28000 for a sample of K-giant members of several open clusters, among which 3 stars in M 67. Iron abundances coming from Fe I lines for such stars are:  $0.03$ ,  $-0.05$  and  $-0.01$  dex. The final result for the cluster that they give, which takes into account also Fe II lines, is  $0.02 \pm 0.14$ .

These results all agree at least reasonably with ours. Finally, the most recent study on M 67, based also on UVES spectra of main sequence stars (Randich et al. 2006), finds  $[\text{Fe}/\text{H}] = 0.03 \pm 0.03$  which matches with our  $0.03 \pm 0.04$ .

As far the other elements are concerned, the comparison with Randich et al. (2006) is also very satisfactory: the discrepancies are in most cases (aluminum, calcium, titanium and nickel) within 0.02 dex, oxygen and sodium are the only elements that differ by as much as 0.08 and 0.07 dex respectively. We remind here that we have used the same line list but different synthesis code and model atmosphere as Randich et al. (2006).

Results by Yong et al. (2005), despite the match of the iron abundance value, point to abundance ratios systematically higher than ours. The disagreement is twice as large as their quoted rms errors, or more, as in the cases of aluminum, sodium and titanium.

Our conclusion is that all recent studies agree well, indicating a remarkable similarity in the M 67 iron content, and in most cases they agree on a chemical composition similar to the solar one. Yet, there are some disagreement in some element abundances, aluminum and sodium being the worst cases. We notice here that for these two elements the abundances rely only on few lines, and that Yong et al. (2005) analysis is based on giant stars. For them discrepancy between dwarfs and giants of the same cluster is often found (see e.g. Randich et al. 2006).

#### 4.3.4. Praesepe

Former studies give for this cluster metallicities either barely supersolar or sensibly supersolar. Our result belongs to the latter group. Boesgaard & Budge (1988) used high resolution spectra ( $0.1\text{--}0.2 \text{ \AA}$ ) of five F dwarfs and one spectroscopic binary taken at the Palomar 5-meter Hale telescope, and they obtain  $+0.13 \pm 0.07$ . Boesgaard (1989) reanalysed three of the five Praesepe F dwarfs spectra presented in Boesgaard & Budge (1988), selecting those with low rotational velocities and well determined temperatures. They found  $[\text{Fe}/\text{H}]$  values of:  $0.033$ ,  $0.106$  and  $0.147$ , thus leading to a reviewed mean cluster metallicity of  $0.092 \pm 0.067$ . Friel & Boesgaard (1992) also measured Praesepe's mean metallicity. Their

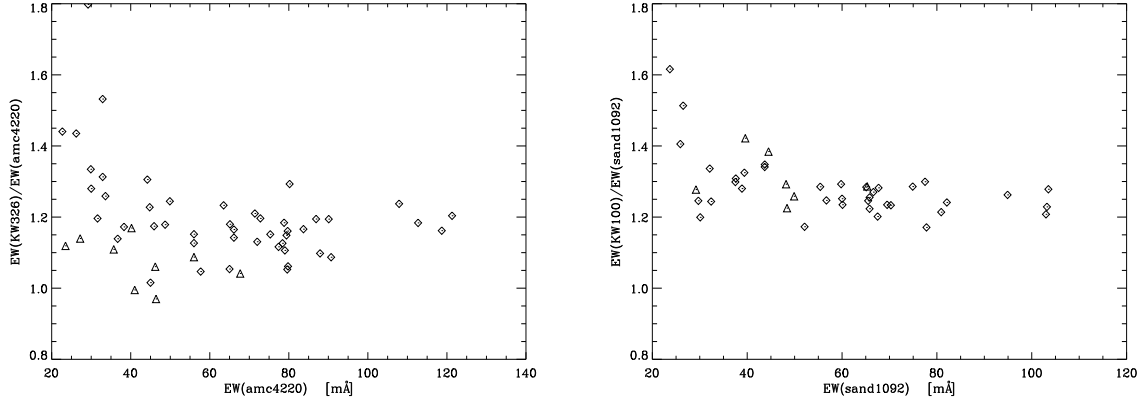


**Fig. 1.** Comparisons between iron line EW measurements of stars with different abundances and with similar (spectroscopic) temperatures. Two Praesepe stars are compared respectively with a star in IC 4651 (KW 326 vs. AMC 4220, left panel) and in M 67 (KW 100 vs. Sanders 1092, right panel). Fe I and FeII lines are plotted with different symbols. KW 100 and Sanders 1092 have virtually the same temperature. AMC 4220 is evaluated to be about 100 K hotter than KW 326, which reduces the effect of the metallicity difference on the EW ratios between the two stars.

result is  $[\text{Fe}/\text{H}] = 0.038 \pm 0.039$ . They had two stars in common with Boesgaard (1989), for which the result agreed very well (0.033 and 0.016 dex of difference in the measurements). The disagreement with our  $[\text{Fe}/\text{H}] = 0.27$  is quite apparent in this case.

For this cluster An et al. (2007) obtain from spectroscopy a moderate supersolar metallicity ( $[\text{Fe}/\text{H}] = 0.11 \pm 0.03$  dex) which is the adopted value, but they find a higher result from photometric analysis ( $[\text{Fe}/\text{H}] = 0.20 \pm 0.04$  dex), both adopting published reddening and by means of simultaneous parameter determination.

Figure 1 shows a comparison between iron line EW measurements in one Praesepe star and, respectively, one star in IC 4651 (left panel) and one in M 67 (right panel). For the comparison we have chosen pair of stars whose temperatures, as derived in the spectral analysis, differ for only 110 K and 10 K respectively: KW 326 vs. AMC 4220 in the left panel, and KW 100 vs. Sanders 1092. The differences between the EWs are of about 15% between KW 326 and AMC 4220 and even more between KW 100 and Sanders 1092.

Furthermore, we have repeated the chemical analysis of Praesepe stars by using two more different combinations of parameters in addition to the adopted ones. First we have used the values computed in Section 3, namely  $T_{\text{phot}}$ ,  $G_{\text{phot}}$  and  $\xi_{\text{fit}}$ . Then the combination of parameters that most flatten the EW and  $\chi$  vs. abundance trend, with no regards on photometric or any other kind of constraints, i. e. the parameters obtained by means of the spectral analysis before finally adjusting them to better match with  $T_{\text{phot}}$ ,  $G_{\text{phot}}$  and  $\xi_{\text{fit}}$  (see again Section 3)

In both cases, and for each and every star, the abundance analysis confirms a high metallic content for the cluster, as can be seen in Table 7. We can confidently conclude Praesepe shows an enhanced average metallicity not lower than  $\approx 0.2$  dex, which makes its similarity to the Hyades even more than what thought in the past (See also Section 5).

star	[Fe/H]	$\xi$	T	G	ion. eq.	corr( <i>chi</i> vs.ab)	corr(EW vs.ab)
$T = T_{phot}, G = G_{phot}, \xi = \xi_{fit}$							
KW 49	0.220	1.15	6028	4.44	-0.11	0.35	0.62
KW 100	0.354	1.09	5977	4.45	-0.30	0.10	0.76
KW 208	0.202	1.11	5993	4.45	-0.22	0.44	0.54
KW 326	0.447	0.98	5873	4.47	0.07	-0.10	0.54
KW 368	0.409	0.91	5811	4.48	0.12	-0.36	0.59
KW 392	0.246	1.01	5902	4.46	-0.27	0.39	0.47
KW 418	0.187	1.19	6062	4.44	-0.16	0.48	0.40
Minimising parameters with very loose photometric constraints							
KW 49	0.268	1.58	6290	4.66	0.01	0.01	0.01
KW 100	0.409	1.76	6370	4.64	-0.01	-0.22	0.05
KW 208	0.322	1.52	6340	4.64	0.00	-0.01	-0.02
KW 326	0.366	1.14	5860	4.62	-0.01	-0.06	0.10
KW 368	0.166	1.34	5700	4.52	0.00	-0.03	0.04
KW 392	0.354	1.44	6250	4.60	0.00	0.01	0.02
KW 418	0.359	1.44	6450	4.76	0.00	0.00	0.03

**Table 7.** Abundance analyses remade for Praesepe stars. In the upper part of the Table theoretical parameters are used (temperature from the photometry, gravity from the models and the temperature, microturbulence from the fit). In the lower part of the Table time we adopted the best parameters found ignoring constraints from photometry or models. Also these analyses confirm the high metallicity of Praesepe is evident.

#### 4.4. Comparison between photometric and spectroscopic temperatures

In Table 8 we show the photometry adopted, together with the stellar parameters derived from it and the spectroscopic parameters. The mean  $T_{spec} - T_{phot}$  values are 120, 325, 122 and 169 K for NGC 3680, IC 4651, Praesepe and M 67 respectively. With the exception of two Praesepe stars, the photometric temperature is always lower than the spectroscopic one. Praesepe suffers little extinction, and its mean  $T_{spec} - T_{phot}$  value is, together with NGC 3680, the lowest one. But it is also the only cluster for which the stellar values of this quantity are very dispersed around the average, which is not surprising, since, as discussed in Section 4.1.2, more problems arose in the determination of the spectroscopic parameters for Praesepe stars. The systematic bias towards positive  $T_{spec} - T_{phot}$  has three possible causes: errors in the colour-temperature transformation, errors in the adopted cluster reddening, some systematic effect in determining the spectroscopic temperature. Since the error in the clusters' extinction depends on the cluster, the other sources of systematic errors should affect all the stars in a similar way. All the clusters have a similar average  $T_{spec} - T_{phot}$  but IC 4651, for which this quantity is  $\approx 150$  K higher than in M 67 and  $\approx 200$  K higher than in the two other clusters. It is natural to suggest that this is due to an underestimation of the B-V colour excess adopted for IC 4651 (Anthony-Twarog & Twarog 1987). If this is the case, a value about 0.04 higher, i.e.  $E(B-V)$  between 0.12 and 0.13 mag, is the correct one. Similar conclusions were obtained by Pasquini et al. (2004) and Biazzo et al. (2007).



STAR	PHOTOMETRY				COMPUTED		SPECTROSCOPIC		
	2MASS		Johnson		VALUES		VALUES		
	J	H	K <sub>S</sub>	V	$T_{eff}$	$\log G$	$T_{eff}$	$\log G$	$\xi$
NGC 3680									
AHTC 1009	13.094	12.813	12.730	14.290	5926	4.46	6010	4.50	1.16
Eggen 70	13.471	13.157	13.088	14.589	6053	4.44	6210	4.47	1.36
IC 4651									
AMC 1109	13.153	12.805	12.773	14.534	5678	4.50	6060	4.55	1.20
AMC 2207	13.210	12.931	12.831	14.527	5824	4.48	6050	4.36	1.18
AMC 4220	13.551	13.215	13.088	14.955	5605	4.51	5910	4.57	1.06
AMC 4226	13.303	12.966	12.909	14.645	5743	4.49	5980	4.44	1.19
Eggen 45	12.961	12.657	12.617	14.27	5844	4.47	6320	4.43	1.50
PRAESEPE									
KW 49	9.591	9.330	9.276	10.65	6028	4.44	6150	4.50	1.41
KW 100	9.463	9.242	9.182	10.57	5977	4.45	6150	4.34	1.78
KW 208	9.565	9.357	9.259	10.66	5993	4.45	6280	4.58	1.52
KW 326	10.091	9.784	9.706	11.20	5873	4.47	5800	4.48	1.28
KW 368	10.183	9.825	9.753	11.30	5811	4.48	5720	4.49	1.12
KW 392	9.659	9.396	9.329	10.78	5902	4.46	6250	4.56	1.48
KW 418	9.463	9.227	9.142	10.51	6062	4.44	6150	4.36	1.27
M 67									
Sand 746	13.058	12.746	12.628	14.380	5608	4.41	5750	4.43	0.84
Sand 1048	13.189	12.856	12.804	14.411	5792	4.36	5900	4.37	0.94
Sand 1092	13.189	12.856	12.804	13.308	5960	4.32	6160	4.41	1.42
Sand 1255	13.216	12.921	12.844	14.486	5733	4.38	5840	4.48	1.05
Sand 1283	12.926	12.630	12.599	14.115	5903	4.33	6100	4.41	1.16
Sand 1287	12.835	12.503	12.442	14.030	5838	4.35	6100	4.41	1.26

**Table 8.** Comparison between spectroscopic and computed values, i.e. photometric temperatures and gravities computed assuming photometric temperatures. The photometric temperatures are computed by means of the infrared magnitudes from the 2MASS catalogue (shown in the second, third and fourth Column) which have been converted into TCS colours, together with the available V magnitudes (shown in fifth Column).

#### 4.5. Summary

For most of the elements and all of the clusters, our results point out to, or are at least consistent with, solar scaled abundances for all of the four target clusters, no matter whether considering  $\alpha$  elements (oxygen, silicon, calcium and titanium), iron-peak elements (iron, chromium and nickel), or the odd- $Z$  elements aluminum and sodium. Among the few elements that represent an exception, the most notable one is the oxygen which, at odds with the other  $\alpha$  elements, is 0.4 dex below its solar-scaled value in Praesepe and 0.2 higher in NGC 3680. Undersolar (slightly beyond the errors) are also aluminum in NGC 3680 and IC 4651, and nickel in NGC 3680.

## 5. The metallicity gradient and the age-metallicity relationship.

The comparisons of our metallicity measurements with other high-quality data analyses made in Section 4.4, clearly shows that these studies agree within the quoted errors even when they employ different model atmospheres and methods of analysis. In Table 9 we compile all the open cluster abundance measurements to our knowledge, obtained using high-resolution spectroscopic analysis. For our target clusters, abundance data and relative errors are taken from the present work, regardless whether or not other results are also available. For M 67 and IC 4651 our results are, however, almost indistinguishable from the mean literature value. For Collinder 261, Berkeley 29 and NGC 6253 we give the average of the two determinations in Table 6 and half of the differences between them as, respectively, abundance estimation and relative error. The results are shown along with the references, the instruments used and their spectral resolution. Clusters' ages and Galactocentric distances are also given. For the latter values, in the cases in which we used the WEBDA database, we adopted the distance and the Galactic coordinates from the database, and assumed a solar distance from the Galactic center of 8 Kpc, for homogeneity with Bragaglia & Tosi (2006).

We have reported only one study on Hyades cluster, i.e. Paulson et al. (2003), a very extensive one (almost one hundred target stars) which give  $[\text{Fe}/\text{H}] = 0.13 \pm 0.05$  dex. The history of the metallicity measurements for Hyades is nicely summarised in Takeda (2008) (see Figure 8 therein): they range from  $\approx 0.1$  to  $\approx 0.2$  dex, Takeda's analysis favouring the higher results.

The other element abundance ratios given in Paulson et al. (2003) are solar within  $1\sigma$ , further stressing the similarity between Hyades and Praesepe.

The abundance data and the Galactocentric distances in Table 9 have been displayed in the Galactocentric-distance vs. metallicity diagram of Figure 2. The Hyades abundance used in such Figure is 0.16 dex, with an error bar of 0.04 dex, in order to take into account both the aforementioned Paulson et al.'s result (0.13 dex), and the higher estimations at around 0.2 dex given by other authors. Error bars on the x-axis are difficult to evaluate, and it would be premature at this stage to push the statistical analysis too further, but they can easily reach several Kpc for the most distant clusters. A homogeneous and reliable photometry and open cluster parameter determination is as much important as the robustness of the metallicity measurements. Of the four datapoints from this work in Figure 2, only Praesepe significantly departs above the -0.06-dex/Kpc-steep linear fit. The only two other clusters which show an exceptionally high iron content are the very metal rich NGC 6253 and NGC 6791, whose abundances are also solar scaled for most of the elements (Sestito et al. 2007; Carretta et al. 2007). Anyway, these three clusters are very different one another as far age as and location are concerned. In particular the relatively young and close by Praesepe has not formed significantly inner in the Galactic Disk and drifted outwards later on, as suggested for NGC 6791 (Carretta et al. 2007).

It is worth of mention that the most metal rich clusters so far analysed, NGC 6253 and NGC 6791, to which we add Praesepe, are all very underabundant in oxygen, which may lead us to think that they formed out of material enriched by type Ia supernovae. But this

suggestion is not supported by the abundance ratios of the other alpha elements, which are overall solar.

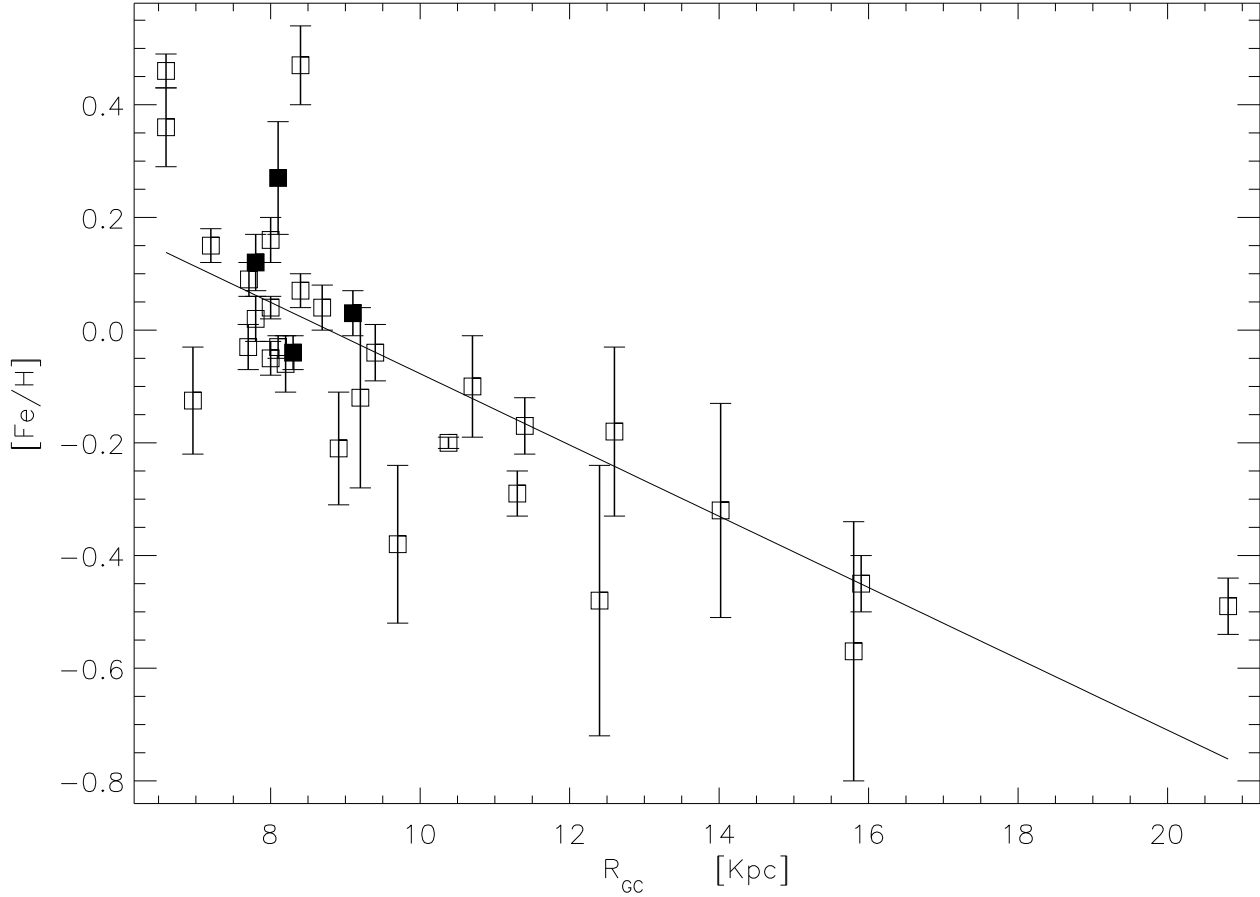


**Fig. 2.** Abundance gradient as resulting from high-spectroscopy open cluster chemical analyses. Data plotted and relative errorbars are as in Table 9, only for Hyades we have adopted in this Figure a different value, i.e.  $0.16 \pm 0.04$  dex, which takes into account also other estimations at about 0.2 dex. The y-axis of the filled symbol points refer to our datapoints. The line represents the  $-0.06$  dex/Kpc relation.

## 6. Conclusions.

This work is one of several aimed at collecting high-precision abundance measurements in open clusters, based on high-resolution and high-signal-to-noise spectra. We present data for four clusters, and we confirm all the abundance trends present in the recent literature for IC 4651 and M 67. For these clusters all the recent determinations agree within a few hundredths of dex, irrespective of whether dwarfs or giants have been observed. We report slightly different abundances for NGC 3680 and mostly Praesepe, which is shown to be substantially metal rich.

The modern iron determinations agree very well in most of the cases, though there is still no precise agreement on how much Praesepe and Hyades are supersolar. Metallicity measurements for open clusters are becoming consistent, independent of the group and of the analysis carried over. As for abundance ratios of elements other than iron, significant differences between results from different groups still arise.

The dispersion within each cluster is limited to a few hundredth of dex, and differences up to 0.1 dex or more are measured between the single objects. These differences have to be interpreted as due to limitations in the observations and in the analysis rather than real, intrinsic chemical variations in the cluster composition. Some caution should therefore be present when adopting analyses which consider only one or a few stars/cluster, if accurate results are pursued.

We find a significant supersolar metallicity for IC 4651 ( $[\text{Fe}/\text{H}]=0.12\pm0.05$ ), a solar metallicity for M 67 ( $[\text{Fe}/\text{H}]=0.03\pm0.04$ ) and a slight undersolar metallicity for NGC 3680 ( $[\text{Fe}/\text{H}]=-0.04\pm0.03$ ). The surprising result is that of Praesepe, as metal rich as  $[\text{Fe}/\text{H}]=0.27\pm0.10$ . The photometric analysis in An et al. (2007) also indicates that Praesepe is metal rich. The reasons of the discrepancy with other results need to be further investigated.

As far as other elements, the composition is solar within the errors for all of them and for all the clusters, except for aluminum (subsolar in NGC 3680 and IC 4651), nickel (also subsolar in NGC 3680) and oxygen. As for the latter, we find  $[\text{O}/\text{Fe}]$  to be  $\approx 0.2$  and  $\approx -0.4$  in NGC 3680 and Praesepe respectively, and just  $\approx 1\sigma$  below the solar value in M 67.

We confirm the extraordinary similar overall chemical composition of the Sun and M 67.

*Acknowledgements.* We are greatly indebted to Sofia Randich for her contribution to the data analysis presented here and for many useful comments. Jorge Melendez, Nuno Santos, Valentina D’Orazi and K. Sinha deserve to be warmly thanked for their valuable feedback. Data collected at ESO, VLT. This publication made use of data products from the Two Micron All Sky Survey, which is a joint project of the University of Massachusetts and the Infrared Processing and Analysis Center/California Institute of Technology, funded by the National Aeronautics and Space Administration and the National Science Foundation; and from the WEBDA database, created by J.-C. Mermilliod and now operated at the institute for Astronomy of the University of Vienna. The SIMBAD astronomical database and the NASA’s Astrophysics Data System Abstract Service have also been extensively used. G. P. acknowledges the support of the project PTDC/CTE-AST/65971/2006 of the Portuguese FCT and that of Indian DST, L. P. acknowledges ESO DGDF.

## References

- Allende Prieto, C., Lambert, D. L., & Asplund, M. 2001, *ApJ*, 556, L63
- An, D., Terndrup, D. M., Pinsonneault, M. H., Paulson, D. B., Hanson, R. B., & Stauffer, J. R. 2007, *ApJ*, 655, 233
- Anthony-Twarog, B. J., Mukherjee, K., Twarog, B. A., & Caldwell, N. 1988, *AJ*, 95, 1453
- Anthony-Twarog, B. J., & Twarog, B. A. 1987, *AJ*, 94, 1222
- Anthony-Twarog, B. J., & Twarog, B. A. 2004, *AJ*, 127, 1000
- Barrado y Navascués, D., Deliyannis, C. P., & Stauffer, J. R. 2001, *ApJ*, 549, 452
- Biazzo, K., et al. 2007, *A&A*, 475, 981
- Boesgaard, A. M. 1989, *ApJ*, 336, 798
- Boesgaard, A. M., & Budge, K. G. 1988, *ApJ*, 332, 410
- Bragaglia, A., Gratton, R. G., Carretta, E., Clementini, G., Di Fabrizio, L., & Marconi, M. 2001, *AJ*, 122, 207
- Bragaglia, A., Sestito, P., Villanova, S., Carretta, E., Randich, S., & Tosi, M. 2008, *A&A*, 480, 79
- Bragaglia, A., & Tosi, M. 2006, *AJ*, 131, 1544
- Carraro, G., & Chiosi, C. 1994, *A&A*, 287, 761
- Carraro, G., Bresolin, F., Villanova, S., Matteucci, F., Patat, F., & Romaniello, M. 2004, *AJ*, 128, 1676

- Carretta, E., Bragaglia, A., Gratton, R.G., & Tosi, M. 2004, *A&A* 422, 951
- Carretta, E., Bragaglia, A., Gratton, R. G., & Tosi, M. 2005, *A&A*, 441, 131
- Carretta, E., Bragaglia, A., & Gratton, R. G. 2007, *A&A*, 473, 129
- Cayrel, R., Cayrel de Strobel, G., & Campbell, B. 1988, *IAU Symp.* 132: The Impact of Very High S/N Spectroscopy on Stellar Physics, 132, 449
- Chiappini, C., Matteucci, F., & Gratton, R. 1997, *ApJ*, 477, 765
- Chiappini, C., Matteucci, F., & Romano, D. 2001, *ApJ*, 554, 1044
- Dekker, H., D’Odorico, S., Kaufer, A., Delabre, B., & Kotzlowski, H. 2000, *Proc. SPIE*, 4008, 534
- Dias, W. S., & Lépine, J. R. D. 2005, *ApJ*, 629, 825
- Edvardsson, B., Andersen, J., Gustafsson, B., Lambert, D. L., Nissen, P. E., & Tomkin, J. 1993, *A&A*, 275, 101
- Eggen, O. J. 1969, *ApJ*, 155, 701
- Eggen, O. J. 1971, *ApJ*, 166, 87
- Ford, A., Jeffries, R. D., & Smalley, B. 2005, *MNRAS*, 364, 272
- François, P., Matteucci, F., Cayrel, R., Spite, M., Spite, F., & Chiappini, C. 2004, *A&A*, 421, 613
- Friel, E. D., & Boesgaard, A. M. 1992, *ApJ*, 387, 170
- Friel, E. D., Janes, K. A., Tavaréz, M., Scott, J., Katsanis, R., Lotz, J., Hong, L., & Miller, N. 2002, *AJ*, 124, 2693
- Friel, E. D., Jacobson, H. R., Barrett, E., Fullton, L., Balachandran, S. C., & Pilachowski, C. A. 2003, *AJ*, 126, 2372
- Friel, E. D., Jacobson, H. R., & Pilachowski, C. A. 2005, *AJ*, 129, 2725
- Friel, E. D., & Janes, K. A. 1993, *A&A*, 267, 75
- Girardi, L., Bressan, A., Bertelli, G., & Chiosi, C. 2000, *A&AS*, 141, 371
- Gratton, R. 2000, *ASP Conf. Ser.* 198: Stellar Clusters and Associations: Convection, Rotation, and Dynamos, 198, 225
- Grevesse, N., & Sauval, A. J. 1999, *A&A*, 347, 348
- Grevesse, N., & Sauval, A. J. 2000, *Origin of Elements in the Solar System, Implications of Post-1957 Observations*, 261
- Hobbs, L. M., Thorburn, J. A., & Rodriguez-Bell, T. 1990, *AJ*, 100, 710
- Hobbs, L. M., & Thorburn, J. A. 1991, *AJ*, 102, 1070
- King, J. R., & Hiltgen, D. D. 1996, *AJ*, 112, 2650
- Klein Wassink, W. J. 1927, *Publications of the Kapteyn Astronomical Laboratory Groningen*, 41, 1
- Johansson, S., Litzén, U., Lundberg, H., & Zhang, Z. 2003, *ApJ*, 584, L107
- Johnson, H. L. 1952, *ApJ*, 116, 640
- Jones, B. F., & Cudworth, K. 1983, *AJ*, 88, 215
- Jones, B. F., & Stauffer, J. R. 1991, *AJ*, 102, 1080
- Kurucz, R. 1993, *ATLAS9 Stellar Atmosphere Programs and 2 km/s grid*. Kurucz CD-ROM No. 13. Cambridge, Mass.: Smithsonian Astrophysical Observatory, 1993., 13,
- Langer, G. E., Fischer, D., Sneden, C., & Bolte, M. 1998, *AJ*, 115, 685
- Latham, D. W., Mathieu, R. D., Milone, A. A. E., & Davis, R. J. 1992, *Evolutionary Processes in Interacting Binary Stars*, 151, 471
- Lawrence, A., et al. 2007, *MNRAS*, 379, 1599
- McPherson, A. M., et al. 2006, *Proc. SPIE*, 6267,
- Meibom, S., Andersen, J., & Nordström, B. 2002, *A&A*, 386, 187
- Modigliani, A., Mulas, G., Porceddu, I., Wolff, B., Damiani, F., & Banse, B. K. 2004, *The Messenger*, 118, 8
- Montgomery, K. A., Marschall, L. A., & Janes, K. A. 1993, *AJ*, 106, 181
- Nordstroem, B., Andersen, J., & Andersen, M. I. 1996, *A&AS*, 118, 407
- Nordstroem, B., Andersen, J., & Andersen, M. I. 1997, *A&A*, 322, 460
- Pace, G., & Pasquini, L. 2004, *A&A*, 426, 1021
- Pasquini, L., Randich, S., & Pallavicini, R. 2001, *A&A*, 374, 1017

- Pasquini, L., Randich, S., Zoccali, M., Hill, V., Charbonnel, C., & Nordström, B. 2004, *A&A*, 424, 951 (15)
- Pasquini, L., Biazzo, K. et al. 2008, *A&A*, submitted
- Paulson, D. B., Sneden, C., & Cochran, W. D. 2003, *AJ*, 125, 3185
- Ramírez, I., & Meléndez, J. 2005, *ApJ*, 626, 465
- Randich, S., et al. 2005, *The Messenger*, 121, 18
- Randich, S., Sestito, P., Primas, F., Pallavicini, R., & Pasquini, L. 2006, *A&A*, 450, 557
- Sanders, W. L. 1977, *A&AS*, 27, 89
- Sestito, P., Bragaglia, A., Randich, S., Carretta, E., Prisinzano, L., & Tosi, M. 2006, *A&A*, 458, 121
- Sestito, P., Randich, S., & Bragaglia, A. 2007, *A&A*, 465, 185
- Shen, Z.-X., Jones, B., Lin, D. N. C., Liu, X.-W., & Li, S.-L. 2005, *ApJ*, 635, 608
- Skrutskie, M. F., et al. 2006, *AJ*, 131, 1163
- Sneden, C. 1973, *ApJ*, 184, 839
- Stix, M. 2002, *The sun : an introduction – 2nd ed.* /Michael Stix. Berlin : Springer, 2002. QB 521 .S75,
- Takeda, Y., 2008, *The Metal-Rich Universe*, La Palma, June 2006, edited by G. Israelian and G. Meynet, Cambridge Contemporary Astrophysics Series, in press
- Tautvaišienė, G., Edvardsson, B., Tuominen, I., & Ilyin, I. 2000, *A&A*, 360, 499
- Tautvaišienė, G., Edvardsson, B., Puzeras, E., & Ilyin, I. 2005, *A&A*, 431, 933
- Taylor, B.J. & Joner, M.D. 2002, *AAS* 200, 902
- Villanova, S., Carraro, G., Bresolin, F., & Patat, F. 2005, *AJ*, 130, 652
- Yong, D., Carney, B. W., & Teixeira de Almeida, M. L. 2005, *AJ*, 130, 597

**Table 3.** Table of the computed abundances, all from the neutral–element lines. In the rows with the average the standard deviation refers to the different stellar values within the cluster (for NGC 3680 we give half of the difference between the two stellar values). In the other rows the standard deviations refer to the measurements from the different lines. When no more than 3 lines are used for a given element, half the difference between the largest and the smallest values, rather than the standard deviation, is given. In the case of Praesepe the errors adopted are higher than the standard deviation: 0.10 dex.

STAR	[Fe/H]	N <sub>Fe</sub>	σ <sub>Fe</sub>	[Na/H]	N <sub>Na</sub>	σ <sub>Na</sub>	[Al/H]	N <sub>Al</sub>	σ <sub>Al</sub>	[Si/H]	N <sub>Si</sub>	σ <sub>Si</sub>
NGC 3680												
AHTC 1009	0.00± 0.09	59	0.06	0.04± 0.06	2	0.00	-0.14± 0.05	1	0.00	-0.03± 0.02	8	0.04
Eggen 70	-0.07± 0.09	50	0.06	-0.10± 0.06	3	0.08	-0.11± 0.05	1	0.00	-0.07± 0.03	8	0.05
AVERAGE	-0.04	σ=0.03		-0.03	σ=0.07		-0.12	σ=0.02		-0.05	σ=0.02	
IC 4651												
AMC 1109	0.11± 0.09	57	0.04	0.09± 0.06	3	0.05	0.05± 0.05	2	0.01	0.11± 0.02	9	0.04
AMC 2207	0.13± 0.09	62	0.06	0.06± 0.06	3	0.04	0.04± 0.05	2	0.02	0.11± 0.03	9	0.05
AMC 4220	0.19± 0.09	51	0.05	0.12± 0.07	3	0.07	0.01± 0.05	2	0.00	0.11± 0.02	7	0.03
AMC 4226	0.13± 0.09	61	0.09	0.13± 0.07	3	0.09	0.06± 0.05	2	0.03	0.08± 0.02	8	0.05
Eggen 45	0.05± 0.09	61	0.08	0.02± 0.06	3	0.06	-0.05± 0.05	2	0.08	0.09± 0.03	8	0.02
AVERAGE	0.12	σ=0.05		0.09	σ=0.05		0.02	σ=0.04		0.10	σ=0.02	
PRAESEPE												
KW49	0.22± 0.10	54	0.06	0.17± 0.06	3	0.05	–	–	–	0.21± 0.03	7	0.06
KW100	0.27± 0.10	39	0.04	0.27± 0.06	1	0.00	–	–	–	0.38± 0.04	6	0.12
KW208	0.28± 0.10	56	0.05	0.31± 0.06	2	0.00	0.30± 0.05	1	0.00	0.26± 0.03	7	0.05
KW326	0.29± 0.10	53	0.06	0.23± 0.07	3	0.04	0.26± 0.05	1	0.00	0.29± 0.03	7	0.09
KW368	0.26± 0.11	56	0.07	0.19± 0.07	3	0.05	0.17± 0.05	1	0.00	0.23± 0.03	6	0.07
KW392	0.35± 0.11	55	0.04	0.27± 0.07	3	0.07	0.26± 0.05	2	0.00	0.29± 0.04	8	0.10
KW418	0.24± 0.10	56	0.07	0.15± 0.07	3	0.05	0.11± 0.05	1	0.00	0.20± 0.04	7	0.09
AVERAGE	0.27	σ=0.04*		0.23	σ=0.06		0.22	σ=0.08		0.26	σ=0.06	
M 67												
Sanders 746	0.07± 0.09	51	0.04	0.04± 0.07	3	0.03	0.13± 0.05	1	0.00	-0.05± 0.02	6	0.03
Sanders 1048	0.03± 0.10	63	0.06	0.00± 0.06	3	0.03	-0.04± 0.05	2	0.02	-0.01± 0.02	6	0.03
Sanders 1092	0.07± 0.09	59	0.04	0.09± 0.06	3	0.04	0.02± 0.05	2	0.00	0.08± 0.03	9	0.08
Sanders 1255	0.01± 0.10	59	0.04	0.00± 0.07	3	0.05	–	–	–	0.02± 0.02	7	0.06
Sanders 1283	0.03± 0.09	59	0.04	0.04± 0.06	3	0.02	-0.12± 0.05	2	0.00	0.03± 0.03	8	0.08
Sanders 1287	-0.04± 0.09	51	0.03	-0.08± 0.06	3	0.05	–	–	–	-0.05± 0.03	5	0.04
AVERAGE	0.03	σ=0.04		0.01	σ=0.06		0.00	σ=0.10		0.00	σ=0.05	



Table 3 cont.

STAR	[Ca/H]	N <sub>Ca</sub>	$\sigma_{Ca}$	[Ti/H]	N <sub>Ti</sub>	$\sigma_{Ti}$	[Cr/H]	N <sub>Cr</sub>	$\sigma_{Cr}$	[Ni/H]	N <sub>Ni</sub>	$\sigma_{Ni}$
<b>NGC 3680</b>												
AHTC 1009	0.05± 0.08	9	0.02	0.06± 0.11	9	0.03	0.00± 0.12	5	0.05	-0.08± 0.06	21	0.05
Eggen 70	-0.05± 0.08	9	0.03	-0.06± 0.09	9	0.06	-0.05± 0.11	6	0.03	-0.10± 0.07	23	0.06
AVERAGE	0.00	$\sigma=0.05$		0.00	$\sigma=0.06$		-0.03	$\sigma=0.03$		-0.09	$\sigma=0.01$	
<b>IC 4651</b>												
AMC 1109	0.14± 0.08	11	0.04	0.13± 0.11	11	0.05	0.15± 0.11	6	0.04	0.11± 0.06	22	0.05
AMC 2207	0.17± 0.08	11	0.05	0.05± 0.10	10	0.04	0.14± 0.11	6	0.05	0.10± 0.07	23	0.06
AMC 4220	0.19± 0.08	11	0.07	0.17± 0.11	10	0.08	0.21± 0.12	6	0.05	0.17± 0.06	22	0.07
AMC 4226	0.19± 0.08	11	0.08	0.10± 0.11	7	0.08	0.06± 0.11	6	0.08	0.10± 0.06	21	0.08
Eggen 45	0.08± 0.08	11	0.04	0.04± 0.09	10	0.06	0.02± 0.10	6	0.06	0.01± 0.07	19	0.08
AVERAGE	0.16	$\sigma=0.04$		0.10	$\sigma=0.05$		0.12	$\sigma=0.07$		0.10	$\sigma=0.06$	
<b>PRAESEPE</b>												
KW 49	0.19± 0.09	10	0.05	0.19± 0.11	8	0.05	0.19± 0.13	6	0.04	0.22± 0.07	17	0.05
KW 100	0.29± 0.10	5	0.07	0.18± 0.11	4	0.02	0.21± 0.12	3	0.04	0.25± 0.07	10	0.05
KW 208	0.31± 0.09	10	0.10	0.28± 0.11	7	0.05	0.35± 0.12	5	0.03	0.26± 0.07	17	0.07
KW 326	0.26± 0.10	7	0.02	0.28± 0.13	10	0.07	0.28± 0.14	5	0.05	0.26± 0.07	18	0.07
KW 368	0.26± 0.10	9	0.05	0.21± 0.14	8	0.06	0.31± 0.14	6	0.01	0.25± 0.06	20	0.05
KW 392	0.35± 0.09	10	0.07	0.34± 0.11	9	0.06	0.38± 0.13	6	0.05	0.33± 0.08	23	0.05
KW 418	0.25± 0.09	10	0.08	0.13± 0.11	7	0.03	0.26± 0.13	5	0.03	0.20± 0.08	20	0.04
AVERAGE	0.27	$\sigma=0.05$		0.23	$\sigma=0.07$		0.28	$\sigma=0.07$		0.25	$\sigma=0.04$	
<b>M 67</b>												
Sanders 746	0.12± 0.08	11	0.05	0.06± 0.12	11	0.05	0.15± 0.12	6	0.09	0.00± 0.05	15	0.03
Sanders 1048	0.09± 0.08	10	0.05	0.04± 0.11	9	0.03	0.11± 0.12	6	0.04	0.05± 0.06	21	0.06
Sanders 1092	0.11± 0.08	11	0.04	0.13± 0.10	11	0.06	0.08± 0.11	6	0.06	0.07± 0.07	20	0.06
Sanders 1255	0.03± 0.08	10	0.05	-0.01± 0.11	10	0.06	0.04± 0.12	6	0.06	0.04± 0.06	23	0.06
Sanders 1283	0.06± 0.08	11	0.06	0.00± 0.10	10	0.05	0.02± 0.11	5	0.04	0.02± 0.07	22	0.04
Sanders 1287	-0.05± 0.08	11	0.03	-0.16± 0.10	8	0.03	-0.07± 0.11	5	0.07	-0.10± 0.07	22	0.06
AVERAGE	0.06	$\sigma=0.06$		0.01	$\sigma=0.10$		0.06	$\sigma=0.08$		0.01	$\sigma=0.06$	

**Table 9.** Compilation of high-resolution studies on open clusters. The first panel shows the results of the abundance analyses, while the second one summarizes dataset and clusters’ properties, showing, in the given order, the number of stars used, the reference (i.e. number in the bibliography and ”PPF” for the present study; some of the cited references for the abundances are compilations of the results obtained by the same group), the spectral resolution power, the instrument and/or the telescope employed, clusters’ Galactocentric distances and ages. The two latter values are flagged with a letter according to the reference used: F for Friel & Janes (1993), B for Bragaglia & Tosi (2006), C for Carraro & Chiosi (1994) and W for the WEBDA database.

Cluster	[Fe/H]	[O/Fe]	[Al/Fe]	[Ni/Fe]	[Na/Fe]	[Si/Fe]	[Ca/Fe]	[Ti/Fe]
$\alpha$ Per	-0.06 $\pm$ 0.05	–	–	–	–	–	–	–
Be 17	-0.10 $\pm$ 0.09	0.00 $\pm$ 0.05	0.25 $\pm$ 0.09	0.02 $\pm$ 0.09	0.37 $\pm$ 0.08	0.30 $\pm$ 0.05	-0.04 $\pm$ 0.03	-0.1 $\pm$ 0.08
Be 20	-0.45 $\pm$ 0.05	0.18 $\pm$ 0.05	0.18 $\pm$ 0.01	-0.02 $\pm$ 0.02	0.2 $\pm$ 0.1	0.05 $\pm$ 0.03	0.08 $\pm$ 0.01	0.38 $\pm$ 0.06
Be 22	-0.32 $\pm$ 0.19	–	0.28 $\pm$ 0.05	0.04 $\pm$ 0.01	0.04 $\pm$ 0.05	-0.04 $\pm$ 0.1	-0.08 $\pm$ 0.02	0.11 $\pm$ 0.1
Be 29	-0.49 $\pm$ 0.05	0.21 $\pm$ 0.02	0.23 $\pm$ 0.03	0.05 $\pm$ 0.06	0.38 $\pm$ 0.01	0.20 $\pm$ 0.02	0.06 $\pm$ 0.04	0.18 $\pm$ 0.16
Be 31	-0.57 $\pm$ 0.23	0.24 $\pm$ 0.08	0.22 $\pm$ 0.13	0.11 $\pm$ 0.12	0.27 $\pm$ 0.10	0.20 $\pm$ 0.14	0.13 $\pm$ 0.05	0.08 $\pm$ 0.09
Be 32	-0.29 $\pm$ 0.04	–	0.11 $\pm$ 0.10	0.00 $\pm$ 0.04	0.12 $\pm$ 0.07	0.12 $\pm$ 0.04	0.07 $\pm$ 0.04	0.02 $\pm$ 0.06
Be 66	-0.48 $\pm$ 0.24	–	0.00 $\pm$ 0.2	0.24 $\pm$ 0.25	0.15 $\pm$ 0.2	–	-0.05 $\pm$ 0.2	0.43 $\pm$ 0.2
Blanco 1	0.04 $\pm$ 0.02	0.02 $\pm$ 0.11	–	-0.18 $\pm$ 0.01	–	-0.09 $\pm$ 0.02	-0.09 $\pm$ 0.02	-0.10 $\pm$ 0.03
Collinder 261	-0.12 $\pm$ 0.09	-0.15 $\pm$ 0.05	0.25 $\pm$ 0.13	0.04 $\pm$ 0.02	0.41 $\pm$ 0.07	0.23 $\pm$ 0.01	-0.01 $\pm$ 0.02	-0.09 $\pm$ 0.02
Coma Ber	-0.05 $\pm$ 0.03	–	–	–	–	–	–	–
Hyades	0.13 $\pm$ 0.05	–	–	–	0.01 $\pm$ 0.09	0.05 $\pm$ 0.05	0.07 $\pm$ 0.07	0.03 $\pm$ 0.05
IC 4651	0.12 $\pm$ 0.05	–	-0.10 $\pm$ 0.06	-0.02 $\pm$ 0.08	-0.03 $\pm$ 0.07	-0.02 $\pm$ 0.05	0.04 $\pm$ 0.06	-0.02 $\pm$ 0.07
IC 4665	-0.03 $\pm$ 0.04	–	–	0.05 $\pm$ 0.13	–	0.09 $\pm$ 0.19	0.03 $\pm$ 0.14	0.21 $\pm$ 0.17
M 35	-0.21 $\pm$ 0.10	–	–	–	–	–	–	–
M 67	0.03 $\pm$ 0.04	-0.07 $\pm$ 0.08	-0.03 $\pm$ 0.11	-0.02 $\pm$ 0.07	-0.02 $\pm$ 0.07	-0.03 $\pm$ 0.06	0.03 $\pm$ 0.07	-0.02 $\pm$ 0.11
NGC 188	-0.12 $\pm$ 0.16	–	–	–	–	–	–	–
NGC 2141	-0.18 $\pm$ 0.15	0.00 $\pm$ 0.06	0.18 $\pm$ 0.07	0.04 $\pm$ 0.11	0.41 $\pm$ 0.04	0.05 $\pm$ 0.19	0.10 $\pm$ 0.04	0.24 $\pm$ 0.11
NGC 2324	-0.17 $\pm$ 0.05	–	0.00 $\pm$ 0.08	-0.09 $\pm$ 0.02	0.31 $\pm$ 0.10	0.06 $\pm$ 0.11	0.15 $\pm$ 0.05	-0.08 $\pm$ 0.03
NGC 2477	0.07 $\pm$ 0.03	–	-0.01 $\pm$ 0.04	0.00 $\pm$ 0.04	0.12 $\pm$ 0.03	0.05 $\pm$ 0.03	-0.01 $\pm$ 0.01	0.01 $\pm$ 0.06
NGC 2506	-0.20 $\pm$ 0.01	–	–	–	–	–	–	–
NGC 2660	0.04 $\pm$ 0.04	–	-0.08 $\pm$ 0.10	-0.03 $\pm$ 0.02	0.12 $\pm$ 0.04	0.00 $\pm$ 0.03	0.04 $\pm$ 0.05	0.00 $\pm$ 0.03
NGC 3680	-0.04 $\pm$ 0.03	0.2 $\pm$ 0.05	-0.08 $\pm$ 0.04	-0.05 $\pm$ 0.03	0.01 $\pm$ 0.08	-0.01 $\pm$ 0.04	0.04 $\pm$ 0.06	0.04 $\pm$ 0.07
NGC 3960	0.02 $\pm$ 0.04	–	-0.06 $\pm$ 0.06	-0.01 $\pm$ 0.03	0.09 $\pm$ 0.03	0.04 $\pm$ 0.05	0.02 $\pm$ 0.03	-0.04 $\pm$ 0.02
NGC 6134	0.15 $\pm$ 0.03	–	–	–	–	–	–	–
NGC 6253	0.41 $\pm$ 0.05	-0.18 $\pm$ 0.06	-0.08 $\pm$ 0.12	-0.01 $\pm$ 0.06	0.21 $\pm$ 0.02	0.05 $\pm$ 0.03	-0.03 $\pm$ 0.01	-0.1 $\pm$ 0.1
NGC 6791	0.47 $\pm$ 0.07	-0.31 $\pm$ 0.08	-0.21 $\pm$ 0.09	-0.07 $\pm$ 0.07	0.13 $\pm$ 0.21	-0.01 $\pm$ 0.10	-0.15 $\pm$ 0.08	0.03 $\pm$ 0.09
NGC 6819	0.09 $\pm$ 0.03	–	-0.07 $\pm$ 0.07	0.01 $\pm$ 0.02	0.47 $\pm$ 0.07	0.18 $\pm$ 0.04	-0.04 $\pm$ 0.06	-0.01 $\pm$ 0.04
NGC 7789	-0.04 $\pm$ 0.05	-0.07 $\pm$ 0.09	0.18 $\pm$ 0.08	-0.02 $\pm$ 0.05	0.28 $\pm$ 0.07	0.14 $\pm$ 0.05	–	-0.03 $\pm$ 0.07
Pleiades	-0.03 $\pm$ 0.02	–	–	–	–	–	–	–
Praesepe	0.27 $\pm$ 0.10	-0.4 $\pm$ 0.2	-0.05 $\pm$ 0.12	-0.02 $\pm$ 0.1	-0.04 $\pm$ 0.12	-0.01 $\pm$ 0.12	0.00 $\pm$ 0.11	-0.04 $\pm$ 0.12
Saurer 1	-0.38 $\pm$ 0.14	0.47 $\pm$ 0.13	0.33 $\pm$ 0.02	0.20 $\pm$ 0.05	0.44 $\pm$ 0.05	0.38 $\pm$ 0.1	0.20 $\pm$ 0.04	0.12 $\pm$ 0.12

Table 9 cont.

Cluster	N	Reference	R	Instr/OBS	R <sub>GC</sub> [Kpc]	Age [Gyr]
$\alpha$ Per	6	9	60&30K	CFHT & Hale	8.2 W	0.07W
Be 17	3	10	25K	KPNO	10.7 W	12 W
Be 20	2	17	28K	KPNO & CTIO	15.9 W	6.0 W
Be 22	2	16	34K	HIRES/KECK	14.02 B	2.40B
Be 29			See Table 6		20.81 B	3.70B
Be 31	1	17	28K	KPNO & CTIO	15.8 W	2.0 W
Be 32	9	4,13	47K	UVES/VLT	11.30 B	6.5 B
Be 66	1	16	34K	HIRES/KECK	12.4 W	5.0 W
Blanco 1	8	8	50K	Anglo/Aus	8.0 W	0.62W
Collinder 261			See Table 6		6.96 B	6 B
Coma Ber	14	9	60K	CFHT	8.0 W	0.4 W
Hyades	98	12	60	HIRES/KECK	8.0 W	0.8 W
IC 4651	4	1	100K	UVES/VLT	7.8 L	1.6 C
IC 4665	18	14	60K	HIRES/KECK	7.7 W	0.43W
M 35	9	2	20K	WIYN/HYDRA	8.91 B	0.18B
M 67	6	1	100K	UVES/VLT	9.1 F	4.8 C
NGC 188	7	11	34K	KPNO	9.2 W	4.3 W
NGC 2141	1	17	28K	KPNO & CTIO	12.6 F	4 F
NGC 2324	7	4	47K	UVES/VLT	11.4 W	0.4 W
NGC 2477	6	4	47K	UVES/VLT	8.4 W	0.7 W
NGC 2506	2	6	48K	FEROS/1.5m	10.38 B	1.70B
NGC 2660	5	4,13	47K	UVES/VLT	8.69 B	0.95B
NGC 3680	2	1	100K	UVES/VLT	8.3 F	1.8 C
NGC 3960	6	4,13	47K	UVES/VLT	7.80 B	1.2 B
NGC 6134	6	6	48K&43K	FEROS/1.5m & UVES/VLT	7.2 W	0.93W
NGC 6253			See Table 6		6.6 B	3 B
NGC 6791	5	7	43K	UVES/VLT	8.4 F	4.4 W
NGC 6819	3	3	40K	SARG/TNG	7.71 B	2 B
NGC 7789	9	15	30K	SOFI/NOT	9.4 F	2 F
Pleiades	13	9	60&30K	CFHT & Hale	8.1 W	0.1 W
Praesepe	7	1	100K	UVES/VLT	8.1 W	0.7 W
Saurer 1	2	5	34K	HIRES/KECK	9.7 W	7.1 W

References. (1)Present study; (2)Barrado y Navascués et al. (2001); (3)Bragaglia et al. (2001); (4)Bragaglia et al. (2008); (5)Carraro et al. (2004); (6)Carretta et al. (2004); (7)Carretta et al. (2007); (8)Ford et al. (2005); (9)Friel & Boesgaard (1992); (10)Friel et al. (2005); (11)Hobbs et al. (1990); (12)Paulson et al. (2003); (13)Sestito et al. (2006); (14)Shen et al. (2005); (15)Tautvaišienė et al. (2005); (16)Villanova et al. (2005); (17)Yong et al. (2005).